Journal of Physics Research and Education, Volume 3, March 2026

A First-Principles Study on Electronic, Magnetic and Optical Properties of Two-Dimensional Janus FeSX (X = Se, Te)

Amretashis Sengupta*

Department of Physics, P.D. Women's College, Jalpaiguri, West Bengal 735101, India

In this work, we study with first-principles methods the electronic material properties of two-dimensional (2D) Janus iron dichalcogenides FeSSe and FeSTe. Using density functional theory (DFT) calculations with the generalized gradient approximation (GGA) and the Perdew-Burke-Ernzerhof (PBE) exchange-correlation functional, we study 2D Janus structures. Structural optimization shows a $P3m1$ structure for the said materials characterized by a central iron layer covalently bonded between two distinct chalcogen layers. Both FeSSe and FeSTe exhibit metallic character with complex, multi-band Fermi surfaces dominated by Fe 3d orbitals and van Hove singularities. A significant finding is the presence of spontaneous magnetization and exchange splitting, confirming magnetically ordered ground states. FeSSe displays a ferromagnetic coupling with a total magnetization of 1.96 μ_B, whereas FeSTe exhibits a quenched magnetic state of 0.47 μ_B due to ferrimagnetic-like tendencies of the Te atoms. Optical calculations show impressive light-harvesting capabilities, with absorption coefficients $1.5 - 1.8{\times}10^6$ cm^{-1} in the ultraviolet region (α_z peaks around $113 - 174$ nm for FeSSe and $114 - 158$ nm for FeSTe) and a broad response extending into the near-infrared to visible region. Furthermore, the inherent structural asymmetry induces a pronounced out-of-plane charge disparity, resulting in an intrinsic electric dipole moment. These findings suggest that 2D Janus Fe-based materials are promising candidates for valleytronics, spintronic injectors, polarization-sensitive photodetectors, catalysis, and the exploration of emergent quantum phases, such as unconventional superconductivity.

I. INTRODUCTION

Janus materials, so named after the Roman deity Janus, which are envisioned to have two faces, typically possess two chemically different surfaces/sides [1–3]. The asymmetry in such material may be in terms of chemical composition of either surface or different functionalization on two sides of the same material [2–4]. Such dissimilar surfaces usually display distinct properties, which make Janus materials interesting in terms of a remarkable mix of electrical, mechanical, and optical capabilities [1–10]. Janus materials are paving the way for advances in an assortment of industries, including electronics, energy storage, and photonics [3–13]. Following the breakthrough of graphene and 2D materials, the concept of Janus materials was extended into the domain of 2D systems as ultra-thin materials with asymmetric exposed surfaces [5–25]. The asymmetry of bulk Janus materials is amplified in these 2D counterparts by completely eliminating inversion symmetry in the out-of-plane direction, which is not possible in conventional Janus particles of other geometries [4]. Consequently, 2D Janus materials not only inherit the unique anisotropy

* amretashis@gmail.com

of their bulk counterparts but also reveal new phenomena driven by quantum confinement and surface-dominated effects, such as enhanced polarization, enhanced catalysis, tuneable electronic structures, and strong coupling between mechanical, electronic, and optical properties [5–25].

Beginning with graphene sheets with distinct surface functionalization [5, 6], a wide range of 2D Janus materials have been studied, such as MoXY [5, 8, 24], WXY [12, 23], SnXY [8, 15]; (X, Y=S, Se, Te), NiXY [13, 14], VSSe [5, 15, 23], PdSSe [9], $HTaSe_2F$ [26], InGaSSe [27], and many more. In addition to 2D Janus transition metal dichalcogenides (TMDCs), many more 2D Janus structures, such as IV-VI Janus materials [28], transition metal trichalcogenides (TMTCs) [29], or other derivatives of TMDCs, such as oxides [30] or oxyhalides [31], have been investigated. The synthesis of such novel materials has drawn on innovative fabrication techniques, such as partial substitution of atoms, especially chalcogens [22], in plasma/LASER-assisted methods [23], thermal exchange reactions [24], or low-energy ion implantation [25], to name a few. Given the constantly expanding landscape of 2D Janus materials, computational methods play a key role in predicting their structures and properties, thereby greatly aiding materials design and discovery.

Recent advancements in the synthesis of iron-based (Fe-based) 2D materials have unlocked new frontiers in the study of strongly correlated electron systems and low-dimensional magnetism. Much interest in this direction is generated by the discovery of hematene (Fe_2O_3) [32], ironene (2D Fe) [33], magnetene (Fe_3O_4) [34] and van der Waals materials such as Fe-Ge-Te [35]. With the possibility of high-temperature superconductivity in monolayer FeSe grown on $SrTiO_3$ substrates [36, 37], research has expanded significantly into metallic and semiconducting iron-chalcogenides and pnictides. Of late more Fe-based chalcogenides such as FeS and FeTe have also been predicted, [38, 39] and more complex Fe-based layered materials such as $Fe_{0.75}TiS_{2-y}Sey$, $KCa_2Fe_4As_4F_2$ are also being studied [40, 41]. These materials, particularly the van der Waals ferromagnet Fe_3GeTe_2 [35], exhibit robust long-range magnetic order that persists down to the monolayer limit, making them ideal candidates for ultrathin spintronic devices and for proximity-effect engineering. The multi-orbital nature of the Fe 3d states within the planar geometry provides the fundamental framework for the intricate coupling of spin, lattice, and orbital dynamics. Consequently, these systems serve as a critical platform for exploring topological superconductivity, quantum phase transitions, and high-efficiency electrocatalysis.

Given the expanding research into 2D Janus materials and the wide-ranging applications of Fe-based 2D materials, it is of great interest to explore 2D Fe-based Janus materials, in particular Fe Janus dichalcogenides. In this study, we propose and examine the characteristics of various Janus 2D Fe dichalcogenide materials using first-principles computations. We suggest Janus FeSSe and FeSTe monolayers with distinct chalcogens on the top and bottom surfaces of their 2D hexagonal structures. We assess the stability, structural characteristics, and electronic, magnetic, and optical properties of the materials being studied using density functional theory simulations.

II. COMPUTATIONAL METHODS

The QUANTUM ESPRESSO code, as implemented in Material Square, is used to perform the density functional theory (DFT) calculations [42–44]. For our computations, we use Perdew-Burke-Ernzerhof (PBE) exchange and correlation with generalized gradient approximation (GGA) DFT [42, 43, 45]. With vacuum cell padding of 10$\mathring{A}$ on each side, a $16 \times 16 \times 1$ Monkhorst-pack $\boldsymbol{k}$-point grid was used to sample the 2D hexagonal unit cells [46]. The cut-off energy for the wave function was chosen to be 60 Ry, and that for the density mesh was taken to be 240 Ry. The calculations were performed using precision pseudopotentials obtained from the Solid-State Pseu-

dopotentials Library (SSSP) precision library, which includes scalar relativistic corrections [47]. For the variable-cell relaxation, the Hellman-Feynmann forces were reduced below 0.01 eV/$\mathring{A}$ and the cell pressure was optimized below 0.02 GPa applying the Broyden-Fletcher-Goldfarb-Shanno (BFGS) algorithm [48, 49]. The formation energy was calculated applying the following formula,

$$E_{BE} = -\left(F_{FeSX} - F_{Fe} - E_S - E_X\right) \tag{1}$$

where E_{FeSX} is the total energy of the 2D FeSX unit cell, E_{Fe}, E_S, and E_X are the total energies of an atom of Fe, S, and X atoms, respectively. E_{BE} is the binding (cohesive) energy. A net positive value from Eq. (1) would suggest a feasible result for the formation of 2D FeSX, taking into account the negative sign of the total energies derived from the DFT calculations. All DFT calculations considered the van der Waals corrections with Grimme's DFT-D3 method [50]. We then proceed to analyze the band structure, density of states, and optical properties of the proposed Janus 2D materials. Spin-polarized DFT calculations were employed for the study of magnetic properties, while the optical properties calculations were carried out with a random phase approximation (RPA) method utilizing the `epsilon.x` package [51] within QUANTUM ESPRESSO [44].

III. RESULTS AND DISCUSSION

The structural configuration of the Janus FeSSe monolayer is derived from the transition-metal dichalcogenide (TMD) framework, specifically adopting a 1T-phase-like coordination in which a central layer of iron (Fe) atoms is covalently bonded between two distinct chalcogen layers. In this asymmetric configuration, one side of the Fe plane is terminated by sulfur (S) atoms, while the opposing side is terminated by selenium (Se) atoms. The optimized lattice parameters are $a = b = 2.962$ $\mathring{A}$ for FeSSe and $a = b = 3.047$ $\mathring{A}$ with a characteristic trigonal angle of γ= 120^o. The substitution of S with Se breaks the out-of-plane mirror symmetry (σh) inherent in symmetric FeS2 or $FeSe_2$ monolayers, effectively reducing the space group symmetry from P$\bar{6}$m2 (or P6$_3$/mmc in bulk) to $P3m1$ (No. 156). The atomic coordinates place Fe at the origin-like z-position, with S and Se occupying the (2/3, 1/3) sites at distinct vertical heights, confirming the sandwich-like trilayer architecture. The in-plane lattice constant a increases in FeSTe to accommodate the larger Te atoms. Interestingly, this expansion causes the Fe-S bond to shorten slightly as the Fe atoms are pulled closer to the S plane to minimize total energy. The difference in bond lengths (Δd) is much more pronounced in FeSTe (0.38 $\mathring{A}$) than in FeSSe (0.12 $\mathring{A}$). The binding energies were calculated to be 1.31 eV for FeSSe and 1.09 eV for FeSTe. Both materials utilize a 1T-like coordination environment. While FeSSe is expected to be relatively stable, FeSTe often exhibits lower thermal stability due to the large atomic radius mismatch between Sulfur and Tellurium, which can lead to structural strain. The calculated band structure of the two Janus materials is presented in Fig. 2. Analysis of the energy dispersions shows a metallic character for both the FeSSe and FeSTe systems. Crossover of multiple bands across the Fermi level indicates a complex, multi-band Fermi surface. Significant band crossings occurring in the vicinity of the gamma point above E_F denote the presence of localized hole pockets. Further, the dispersive bands descending below the Fermi energy along the M-K high-symmetry path and adjacent to the K point correspond to electron pockets. Such multi-orbital metallicity is characteristic of iron-based 2D chalcogenides, where the electronic states near the Fermi level are mostly contributed to by the Fe 3d orbitals. The energy bands corresponding to FeSTe have distinct shifts and altered dispersion curvatures relative to the FeSSe counterpart. Such deviations are attributable to the larger size and less electronegativity

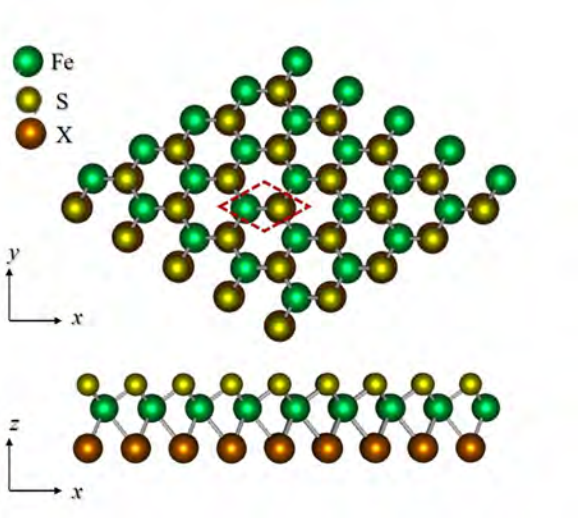

FIG. 1. 2D Janus FeSX structure viewed from the xy and zx planes. The unit cell is highlighted with red dashed lines.

TABLE I. Structural parameters of the optimized 2D Janus materials

Structural Parameter	FeSSe Monolayer	FeSTe Monolayer
Lattice Constant ($a = b$)	2.962 $\mathring{A}$	3.047 $\mathring{A}$
Bond Length (Fe-S)	2.19 $\mathring{A}$	2.17 $\mathring{A}$
Bond Length (Fe-X)	2.31 $\mathring{A}$ (Fe–Se)	2.55 $\mathring{A}$ (Fe–Te)
Bond angle (S-Fe-X)	85.85°	89.82°
Total Thickness (Δz)	3.18 $\mathring{A}$	3.51 $\mathring{A}$

of the Te atom compared to Se, with the more spatially extended 5p orbitals of Te modifying the hybridization strength with the central Fe 3d states. Also, the presence of relatively flat band segments, i.e., regions where the band dispersion is minimal, particularly between the M and K points, suggests the existence of van Hove singularities.

For further understanding of the electronic properties and also exploring the magnetic properties of the Janus FeSSe and FeSTe monolayers, the spin-polarized total density of states (TDOS) and partial density of states were calculated. The density of states results are presented in Fig. 3. A distinct feature in the TDOS profiles of both the 2D Janus materials under study is the clear asymmetry between the spin-up (majority) and spin-down (minority) electronic channels. This pronounced exchange splitting spanning a significant energy range on both sides of the Fermi level confirms that both Janus monolayers possess a spontaneous magnetization, and that they favor a magnetically ordered ground state. Consistent with the calculated band structures, both materials exhibit a finite density of states at the Fermi level, confirming their metallic nature. The unequal DOS at the Fermi level for the two spin channels indicates a high degree of spin polarization at the Fermi energy.

The total magnetization calculated for the FeSSe unit cell was 1.96 μ_B while that for FeSTe was 0.47 μ_B. Elementally for FesSe, the calculated magnetization on the Fe atom was 1.689 μ_B,

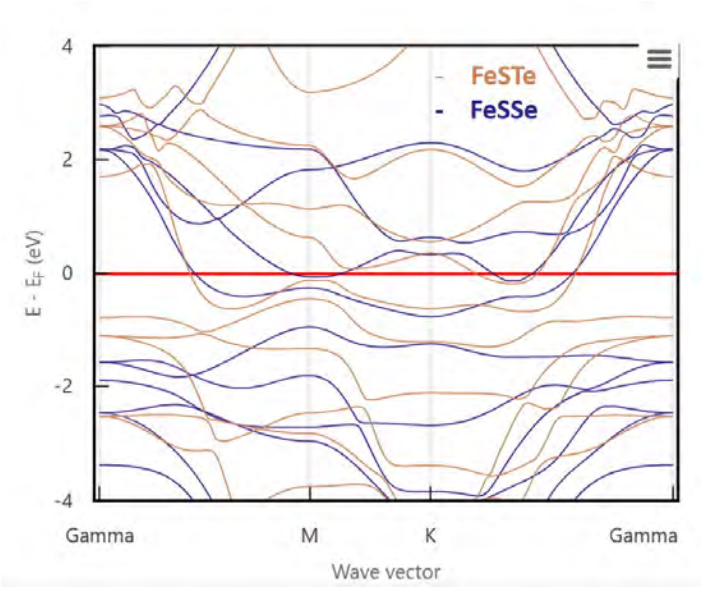

FIG. 2. Calculated bandstructure of the 2D Janus FeSX structure.

while those on the S and Se atoms were 0.053 μ_B and 0.063 μ_B, respectively. Both the S and Se moments being positive indicate a consistent exchange mechanism across the Janus layers. For FeSTe, these values were 0.469 μ_B for Fe, 0.027 μ_B for S, and for -0.011 μ_B for Se . The Te atom showing an antiparallel moment suggests a magnetic frustration or a ferrimagnetic-like tendency with the Te p-orbitals opposing the Fe d-orbitals. Thus, a ferromagnetic coupling between the metal and the ligands in FeSSe and, for FeSTe, a "quenched" magnetic state is observed. The magnetic properties further suggest that such 2D Janus systems could serve as spin-polarized electron injectors, an important component for nanoscale spintronic devices.

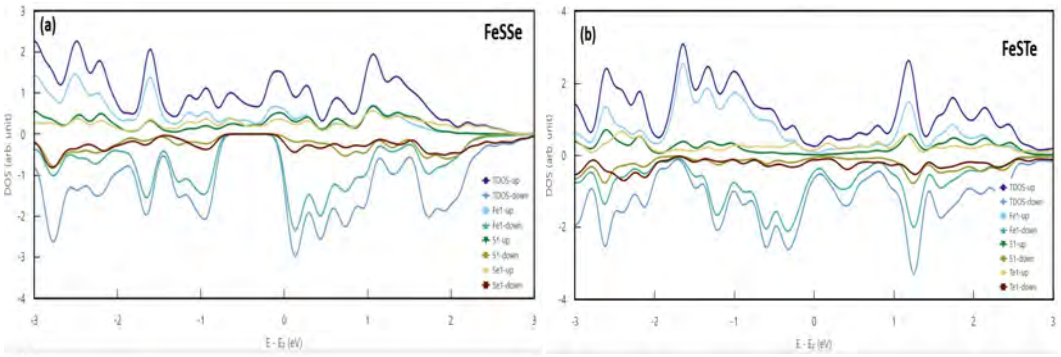

FIG. 3. Calculated density of states (DOS) of the 2D Janus (a) FeSSe and (b) FeSTe structure, showing the total and projected DOS.

Comparing the TDOS of the two monolayers reveal how chalcogen substitution modulates the electronic landscape. While the overall shape of the states remains qualitatively somewhat similar, significant variations occur near the Fermi level. In FeSSe, a sharp, highly localized peak in the

spin-down channel is situated almost immediately above the Fermi level around 0.2 eV. For FeSTe, this prominent minority-spin peak broadens and shifts to higher energies, stabilizing around 1.2 eV. Such upward spectral shift implies that the decreased electronegativity and increased atomic radius of Tellurium significantly alters the crystal field splitting as well as the exchange interaction strength at the central Fe sites. The projected density of states (PDOS) profile shows that the electronic states near the Fermi level, specifically within the energy window -3 eV to $+3$ eV, are predominantly governed by the iron (Fe) 3d orbitals. Furthermore, the exchange splitting between the spin-up and spin-down channels, the primary driver of the spontaneous magnetization, is seen to be almost entirely localized on the Fe atoms. The chalcogen atoms (S, Se, Te) exhibit relatively symmetric spin distributions, confirming that the central Fe layer acts as the primary magnetic center in both Janus architectures. Besides the dominance of Fe atoms in terms of magnetic moment, the role of chalcogen atoms in mediating electronic properties can be better understood by examining covalent hybridization. In the upper valence and lower conduction bands, the projected states of the chalcogen p-orbitals are seen to follow the contour of the Fe 3d states. Such distinct energetic overlap indicates robust p-d covalent hybridization between the central transition metal and the surrounding chalcogen layers. This strong hybridization is a key factor in mediating the magnetic exchange interactions, such as superexchange.

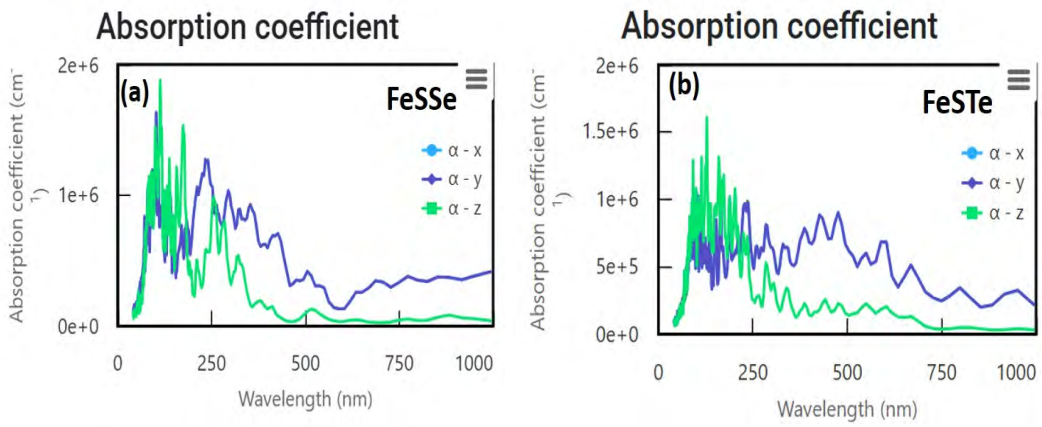

FIG. 4. Calculated absorption spectra of the 2D Janus (a) FeSSe and (b) FeSTe structure.

To evaluate the potential of the 2D Janus iron chalcogenides for optoelectronic applications, the frequency-dependent absorption coefficients (α) of the FeSSe and FeSTe monolayers were calculated. As illustrated in Figs. 4 (a) and 4(b), both Janus monolayers exhibit impressive light-harvesting capabilities, with peak absorption coefficients reaching $1.8\text{x}10^6$ cm^{-1} in the ultraviolet (UV) region. This magnitude is significant for atomically thin materials, indicating strong photon-matter interactions. The strongest peaks for FeSe in α_z is 113 nm, 174 nm, and 158 nm while those for FeSTe are 114 nm, 128 nm, and 158 nm. For the x and y directions, the UV absorption is less than in z-direction for the Janus materials. This UV absorption asymmetry is more distinct for FeSTe than FeSSe. Overall, the x/y absorption peaks in FeSSe are bunched near the 100 nm region, with the peaks with decreasing magnitude in the 237-400 nm region. For FeSTe, the x/y absorption is less in magnitude in the UV region and has a more dispersed, broader profile with peaks of almost similar strength spread out in the 250-500 nm region. The optical anisotropy is observed in the 2D systems under study, stemming from the inherent structural asymmetry of the

Janus geometry. The in-plane absorption components (α_x and α_y) are nearly degenerate, owing to the in-plane structural symmetry of the basal plane. These in-plane components demonstrate a broad spectral response, maintaining significant absorption intensities ($> 10^5$ cm^{-1}) across the visible region and extending deep into the near-infrared (NIR) up to 1000 nm. In stark contrast, the out-of-plane absorption (α_z) is highly localized in the UV regime (approximately 100–300 nm) and decays rapidly at longer wavelengths.

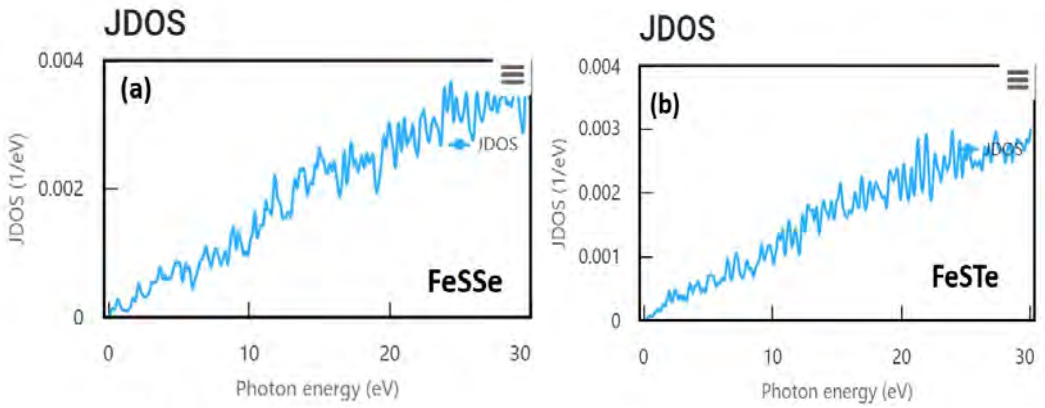

FIG. 5. Calculated joint density of states (JDOS) of the 2D Janus (a) FeSSe and (b) FeSTe structure.

Comparing the two monolayers, we find subtle differences in their optical responses. While FeSSe displays slightly higher peak intensities in the UV range, the FeSTe monolayer exhibits a broader, more diffuse absorption profile in the visible range. Such redshift and broadening can be attributed to the more spatially extended nature of the Te 5p orbitals compared to the Se 4p orbitals, which alters the transition dipole moments and narrows the corresponding energy gaps. To investigate the microscopic origin of these optical features further, we study the joint density of states (JDOS). The JDOS is a measure of the probability of direct interband optical transitions between occupied valence states and unoccupied conduction states. The calculated JDOS for both FeSSe and FeSTe 2D Janus structures are shown in Figs. 5(a) and 5(b). This large number of available transition states at higher photon energies directly correlates with the strong peaks observed in the UV region of the absorption spectra. Also, the low-energy onset of the JDOS, which rises immediately from 0 eV, indicates a dense supply of states near the Fermi level. This continuous abundance of low-energy transitions facilitates the persistent, broadband in-plane absorption in the visible and NIR regions. Quantitatively, the absolute JDOS values are slightly higher for FeSSe compared to FeSTe, which corroborates the relatively higher peak absorption magnitudes observed for the FeSSe monolayer.

The combination of high absorption, strong polarization-dependent optical anisotropy, and broadband in-plane response highlights the significant potential of these 2D Janus structures in optoelectronics. The distinct anisotropies between the in-plane and out-of-plane light harvesting make FeSSe and FeSTe highly promising candidates for ultra-thin, polarization-sensitive photodetectors and next-generation flexible optoelectronic devices. To study the atomistic charge distribution and investigate the asymmetric nature of the Janus monolayers, the charge density profile was studied for the 2D structures. The planar average charge density (ρ) along the out-of-plane direction (z-axis) for both FeSSe and FeSTe is presented in Fig. 6. The charge density (ρ) is expressed in units of e/Bohr³. For both systems, the charge density smoothly decays to zero within

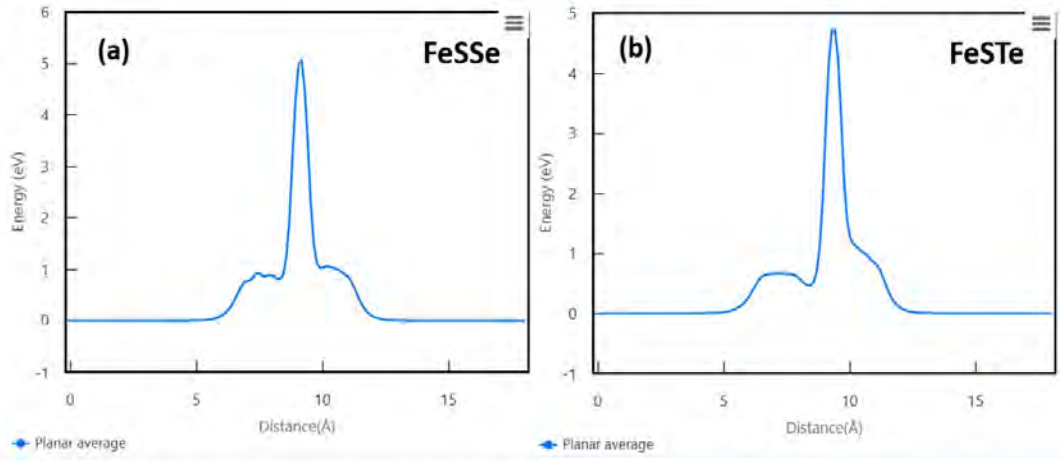

FIG. 6. Charge density projected along the c-axis of the 2D Janus (a) FeSSe and (b) FeSTe structure.

the vacuum regions (0–5 $\mathring{A}$ and 13–18 $\mathring{A}$), confirming that the employed vacuum gap is sufficient to eliminate spurious interactions between adjacent periodic images and properly isolate the 2D slabs. The most prominent feature in both charge density profiles is the sharp, intense central peak located at approximately 9 $\mathring{A}$. This peak corresponds to the strongly localized 3d valence electrons of the central transition metal (Fe) atomic layer. Accompanying this central charge density peak are two distinct shoulder regions associated with the top and bottom chalcogen atomic layers. Unlike pure transition metal dichalcogenides (TMDs), these Janus monolayers exhibit pronounced spatial asymmetry in the shoulder regions due to the differing atomic radii and electronegativities of the out-of-plane chalcogen atoms.

The charge asymmetry in FeSSe between the S and Se layers reflects the differences in the spatial extension of their respective 3p and 4p orbitals. The S atomic plane (right shoulder, 11.0 $\mathring{A}$) displays a local charge density (0.96 e/Bohr^3) while the Se layer (left shoulder, 7.5$\mathring{A}$) shows a charge density of (0.88 e/Bohr^3) This disparity is magnified in the FeSTe owing to the larger physical difference between sulfur and tellurium. The Te atomic plane (left shoulder, 7.5$\mathring{A}$) exhibits a broader, more diffuse charge distribution with a lower local peak density (0.66 e/Bohr^3), characteristic of the highly extended nature of Te 5p orbitals. On the other hand, the S atomic layer (right shoulder, 11.0$\mathring{A}$) displays a narrower spatial profile with a higher local charge density (0.97 e/Bohr^3), corresponding to the more tightly bound and compact S 3p electrons.

Such inherent asymmetry in the out-of-plane charge distribution confirms the non-coincidence of the centers of positive ionic charge and negative electronic charge, leading to a non-zero polarization. This intrinsic out-of-plane electric dipole moment and a built-in electric field across the Janus monolayer can be highly advantageous for modulating band alignments and driving charge carrier separation in photocatalytic and piezoelectric applications, and can be a defining feature for valleytronics. The greater disparity in FeSTe typically results in a significantly stronger intrinsic dipole moment in Te-based Janus materials. The built-in out-of-plane electric field in the Janus structure, combined with spin-orbit coupling (SOC), is expected to induce Rashba-type spin splitting in the electronic bands. Furthermore, the presence of van Hove singularities in the Fe 2D Janus materials is suggested by the flat-band segments observed earlier in the dispersion. The high density of states associated with these topological features often acts as a precursor to electronic

instabilities, making both FeSSe and FeSTe compelling candidates for hosting emergent quantum phases, such as unconventional superconductivity or itinerant magnetism.

IV. CONCLUSION

In summary, this first-principles investigation demonstrates that 2D Janus iron dichalcogenides, FeSSe and FeSTe, are stable monolayers characterized by a unique confluence of metallic, magnetic, and optical properties. By breaking the out-of-plane mirror symmetry inherent in symmetric dichalcogenide structures, these materials adopt a $P3m1$ space group symmetry defined by a central iron layer covalently bonded between distinct chalcogen layers. The electronic analysis reveals that both systems possess a metallic ground state with complex, multi-band Fermi surfaces dominated by Fe 3d orbitals. Notably, the identification of relatively flat band segments indicates the presence of van Hove singularities. Such features are critical, as the associated high density of states often serves as a precursor to emergent quantum phenomena, including unconventional superconductivity or itinerant magnetism.

Magnetically, the Janus geometry induces spontaneous magnetization through pronounced exchange splitting. While FeSSe displays robust ferromagnetic coupling with a total magnetization of $1.96\mu_B$, FeSTe exhibits a "quenched" magnetic state of $0.47\mu_B$ driven by the ferrimagnetic-like tendencies of the Te atoms. This tunable magnetism suggests that these monolayers could serve as highly efficient spin-polarized electron injectors for nanoscale spintronic applications. Furthermore, the inherent structural asymmetry results in a significant out-of-plane charge disparity, producing an intrinsic electric dipole moment and a built-in electric field. This asymmetry is particularly pronounced in FeSTe due to the greater mismatch in atomic radii and electronegativities between Sulfur and Tellurium.

Complemented by impressive light-harvesting capabilities in the ultraviolet region, these materials offer a broad-spectrum optical response and strong polarization-dependent anisotropy. Collectively, these findings position 2D Janus Fe-based materials as a versatile and promising platform for the development of valleytronics, polarization-sensitive photodetectors, and high-efficiency catalysts. Future studies incorporating spin-orbit coupling (SOC) are expected to further elucidate the potential for Rashba-type spin splitting, expanding the utility of these systems in next-generation quantum electronic devices.

Acknowledgments : The author acknowledges the Science and Engineering Research Board (SERB), India, for SERB Research Scientist Fellowship 2020-2022 (Grant No.SB/SRS/2019-20/03/ES).

[1] P. G. de Gennes, Science **256**, 495 (1992).
[2] H. Su *et al.*, Mater. Today Bio **4**, 100033 (2019).
[3] C. K. Söz, S. Trosien and M. Biesalski, ACS Mater. Lett. **2**, 336 (2020).
[4] M. Vafaeezadeh and W. R. Thiel, Angew. Chem. Int. Ed. **61**, e202206403 (2022).
[5] L. Zhang *et al.*, J. Mater. Chem. A **8**, 8813 (2020).
[6] S. W. Ng, N. Noor and Z. Zheng, NPG Asia Mater. **10**, 217 (2018).
[7] A. B. Maghirang *et al.*, NPJ 2D Mater. Appl. **3**, 35 (2019).

[8] L. Ju, M. Bie *et al.*, J. Phys. Mater. **3**, 022004 (2020).
[9] Y. Zhou, X. Yang and J. He, Vacuum **181**, 109649 (2020).
[10] J. Yuan *et al.*, Phys. Rev. B **101**, 094420 (2020).
[11] Z. Kahraman *et al.*, Appl. Surf. Sci. **538**, 148064 (2021).
[12] Y. Fan *et al.*, Sci. Bull. **65**, 27 (2020).
[13] M. Lu *et al.*, ACS Omega **4**, 5714 (2019).
[14] A. Sengupta, Comput. Mater. Sci. **206**, 111278 (2022).
[15] V. Montes-Garcia and P. Samori, Chem. Sci. **13**, 315 (2022).
[16] M. Yagmurcukardes *et al.*, Appl. Phys. Rev. **7**, 011311 (2020).
[17] Y. Zengin and Y. Mogulkoc, Phys. Chem. Chem. Phys. **26**, 16603 (2024).
[18] L. Pan *et al.*, J. Mater. Chem. A **10**, 22676 (2022).
[19] T. V. Vu and N. N. Hieu, J. Phys. Condens. Matter **34**, 115601 (2021).
[20] M. Naseri *et al.*, Physica E **114**, 113581 (2019).
[21] G. Guo *et al.*, Physica E **143**, 115359 (2022).
[22] Y. C. Lin *et al.*, ACS Nano **14**, 3896 (2020).
[23] A. Y. Lu *et al.*, Nat. Nanotechnol. **12**, 744 (2017).
[24] J. Picker *et al.*, Nano Lett. **25**, 3330 (2025).
[25] R. Sant *et al.*, npj 2D Mater. Appl. **4**, 41 (2020).
[26] K. Zheng, T. Vegge and I. E. Castelli, ACS Appl. Mater. Interfaces **16**, 19369 (2024).
[27] M. Chen *et al.*, Research **6**, 0066 (2023).
[28] X. Du and Z. Huang, Front. Phys. **12**, 1534301 (2025).
[29] T. Das and S. Datta, Nanoscale Adv. **2**, 1090 (2020).
[30] J. Dzíbelová *et al.*, Appl. Mater. Today **34**, 101881 (2023).
[31] V. Van Hoang *et al.*, Comput. Mater. Sci. **126**, 446 (2017).
[32] P. Serles *et al.*, Sci. Adv. **7**, eabk2041 (2021).
[33] Y. Deng *et al.*, Nature **563**, 94 (2018).
[34] Q.-Y. Wang *et al.*, Chin. Phys. Lett. **29**, 037402 (2012).
[35] D. Huang and J. E. Hoffman, Annu. Rev. Condens. Matter Phys. **8**, 311 (2017).
[36] Y. Wang *et al.*, Comput. Mater. Sci. **211**, 111523 (2022).
[37] D. Wang, X. Chen and B. Sanyal, Phys. Rev. B **104**, 245410 (2021).
[38] N. V. Selezneva *et al.*, Solid State Sci. **134**, 107049 (2022).
[39] Z. C. Wang *et al.*, J. Am. Chem. Soc. **138**, 7856 (2016).
[40] P. Giannozzi *et al.*, J. Phys. Condens. Matter **21**, 395502 (2009).
[41] P. Giannozzi *et al.*, J. Phys. Condens. Matter **29**, 465901 (2017).
[42] J. P. Perdew, K. Burke and M. Ernzerhof, Phys. Rev. Lett. **77**, 3865 (1996).
[43] H. J. Monkhorst and J. D. Pack, Phys. Rev. B **13**, 5188 (1976).
[44] G. Prandini *et al.*, npj Comput. Mater. **4**, 72 (2018).
[45] C. G. Broyden, J. Inst. Math. Appl. **6**, 76 (1970).
[46] J. D. Head and M. C. Zerner, Chem. Phys. Lett. **122**, 264 (1985).
[47] S. Grimme *et al.*, J. Chem. Phys. **132**, 154104 (2010).
[48] A. Benassi, A. Ferretti and C. Cavazzoni, PWSCF epsilon.x User's Manual.
[49] J. A. Hatchel, The Nanoscale Optical Properties of Complex Nanostructures (Springer, 2018).
[50] J. An *et al.*, Adv. Funct. Mater. **32**, 2110119 (2022).
[51] C. Cui *et al.*, npj 2D Mater. Appl. **2**, 18 (2018).